6

Nematic Ordered Cellulose Templates

Tetsuo Kondo

Graduate School of Bioresource and Bioenvironmental Sciences, Kyushu University, Hakozaki, Higashi-ku, Fukuoka, Japan

CONTENTS

A unique form of β-glucan association, nematic ordered cellulose (NOC), has been developed that is molecularly ordered, yet noncrystalline. NOC has unique characteristics, in particular, its surface properties provide tracks or scaffolds for regulated movements and fiber production of *Gluconacetobacter xylinus* (formerly *Acetobacter xylinum*), which produces cellulose ribbon-like nanofibers 40–60 nm in width and moves due to the inverse force of the secretion of the fibers. Since the interaction

between the produced microbial cellulose nanofibers and specific sites of the oriented molecules on the unique surface of NOC is very strong, such ordered cellulose can be used as a template for the construction of nanocomposites, and the growth direction of the secreted cellulose is controlled by the epitaxial deposition of the microfibrils. Accordingly, the template as a scaffold could regulate and establish deposition of the NOC-patterned three-dimensional (3D) architecture of cellulose ribbon-like nanofibers when the bacteria are incubated on it. This review attempts to reveal the exclusive structure–property relationship in order to extend the use of NOC film as a functional template for bacterium culture and biomimic mineralization. In addition, the other carbohydrate polymers with a variety of hierarchical nematic ordered states on various scales, so called nano-/microstructures, are described, which would allow development of new functional ordered scaffolds. The regulating factors for the rate of the microbial 3D construction are also discussed.

Introduction

Attempts to understand interfacial surface structures and the interaction of materials at the nanoscale have brought us into the field of nanotechnology (Drexler 1992). Microbiological systems combined with nanotechnology have become bionanotechnology (Taton 2002). Recent studies showing the unique interaction of biological systems with entirely synthetic molecular assemblies have prompted consideration of a new generation of approaches for controlled nanoassembly. More recently, we found a unique phenomenon that the molecular tracks of nematic ordered cellulose (NOC) (Kondo 2007; Kondo et al. 2001) substrate regulate the direction of fiber secretion of *Gluconacetobacter xylinus* (formerly *Acetobacter xylinum*), a Gram-negative bacterium that synthesizes and extrudes a cellulose nanofiber, resulting also in regulating the direction of the bacterial movement caused by the inverse force of the secretion. An epitaxial deposition of the nanofibers was induced due to the strong interaction between the nascent nanofibrils and influenced the order of molecules of the template (Kondo 2007; Kondo et al. 2002). This indicated that the conjunction of directed biosynthesis and the ordered fabrication from the nano to the micro scales could lead to new methodologies for the design of functional materials with desired nanostructures.

In the unique phenomenon, the most influential factor for the regulated bacterial movement was the surface of the nano-/microstructure of the template. The NOC substrate, where cellulose molecules are highly ordered but not assembled to form the crystalline state, was prepared by uniaxial stretching of water-swollen and fixed cellulose gel from dimethyl acetamide/LiCl solution. Under wet conditions, the cellulose molecular chains tend to be oriented toward the stretching axis. Simultaneously the hydroxyl (OH) groups

at the C6 position that are equatorially bonded to the anhydroglucose unit in the cellulose molecules are automatically oriented at a certain angle against the surface and also aligned along the same axis as the tracks (Kondo 2007). On the contrary, the lateral order of the OH groups is not well coordinated because of the slipping molecular chains with each other in the NOC that was caused by the uniaxial stretching. Therefore the OH groups tend to be oriented as molecular tracks only in one direction across the entire NOC surface (Kondo 2007; Kondo et al. 2001). These ordering tracks of the OH groups on the NOC surface appear to induce epitaxial deposition of the biosynthesized cellulose nanofibers as they are secreted from *G. xylinus* along the same axis of the tracks in NOC. In addition, the regulated movement of the bacterium was not observed in the synthetic polymers having OH groups such as polyvinyl alcohol (Kondo et al. 2002). Therefore, when the nematic ordered state is prepared using other natural polymers, it is of interest and importance to know whether similar regulated bacterial movement may occur in order to extend this phenomenon into a methodology for fabrication of new types of functional bio-based materials.

In this chapter, after properties of NOC are described, the behavior of cellulose production of two types of *G. xylinus* bacteria (NQ-5, ATCC 53582; and AY-201, ATCC 23769) is at first shown in Hestrin–Schramm media on NOC templates (Hesse and Kondo 2005; Kondo 2007; Kondo et al. 2002). In addition, a modified distribution of carbon isotopes (β-D-glucose-U-$^{13}C_6$) as a precursor for the biological synthesis did not have any influence on the microgravitative effects of the building of cellulose.

Second, we employed chitin and cellulose-chitin blends as the components for the above templates instead of NOC (Kondo et al. 2012). Chitin is a repeating carbohydrate polymer of (1,4)-linked 2-deoxy-2-acetamide-β-D-glucose. That is, as the primary structure, chitin has only a replacement of OH groups into acetamide groups at the C2 position of the anhydroglucose unit when compared with cellulose. However, when treated in the same manner as with NOC, the chitin exhibited a variety of different micro/nano hierarchical nematic ordered states (Kondo et al. 2004). Furthermore, the NOC-like ordered templates of cellulose/cellulose derivative blends were also employed for the bacterial cultures.

Third, as an extended concept for the NOC, attempts are discussed to propose a sort of biomimic mineralization of calcium phosphate using modified NOC templates. This process was initially mediated by the modified NOC template having a pair of roles in the ion supply sources and scaffolds for three-dimensional (3D) ordering architecture of the calcium phosphate as a biomineral (Higashi and Kondo 2012).

This chapter will provide unique surface properties of NOC templates for patterning of the bacterial movement and deposition of their secreted cellulose nanofibers, and patterned deposition of biominerals. Furthermore, the regulated fabrication could lead to the design of 3D architecture from the nano to the micro scales of functional bio-based materials with desired

patterned nanostructures, which also opens pathways toward preparation of potentially versatile organic–inorganic as well as organic–organic order-patterned composites with less energy consumption.

What is NOC?

Prior to NOC, one needs to know the characteristic feature of a cellulose molecule (Figure 6.1): cellulose has an extended structure with a 2_1 screw axis composed of β-1,4 glucosidic linkages between anhydroglucose units. Thus it would be natural to accept the dimer called "cellobiose" as a repeating unit. The three kinds of OH groups within an anhydroglucose unit exhibit different polarities, which contribute to formation of various kinds of inter- and intramolecular hydrogen bonds, including secondary OH at the C2, secondary OH at the C3, and primary OH at the C6 position. In addition, all the OH groups are bonded to a glucopyranose ring equatorially. This causes the appearance of a hydrophilic site parallel to the ring plane. In contrast, the CH groups are bonded to a glucopyranose ring axially, causing a hydrophobic site perpendicular to the ring, as shown in the upper image of Figure 6.1. These effects lead to the formation of hydrogen bonds parallel to the glucopyranose ring, and to van der Waals interactions perpendicular to the ring.

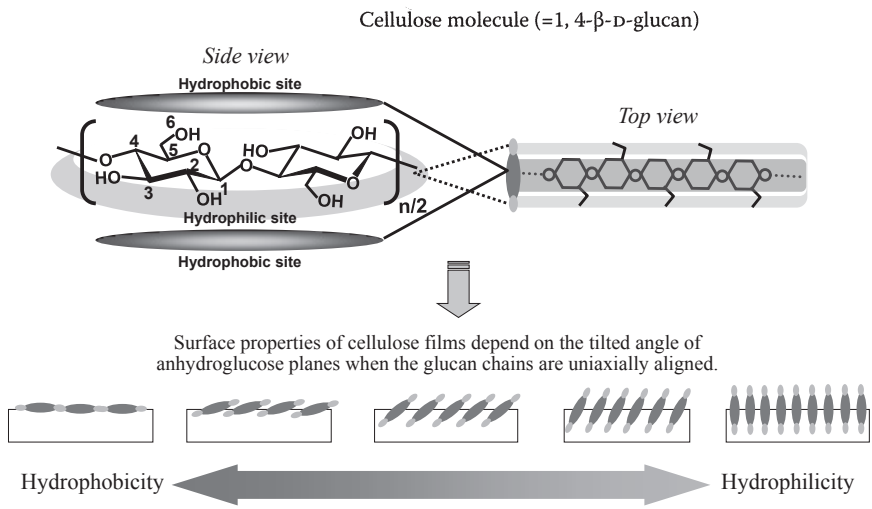

FIGURE 6.1
The site-specific, amphiphilic nature of cellulose chemical structure leading to unique surface properties of cellulose films, depending on the tilted angle of the anhydroglucose planes when the glucan chains are uniaxially aligned.

Another important feature of the OH groups is the type of hydroxymethyl conformation at the C6 position, because the conformation of C5–C6 and the resulting interactions including inter- and intramolecular hydrogen bonds in the cellulose structure may differ from that in crystallites, and also it is assumed to make up the extent of crystallization, as well as the final morphology of cellulose. In the noncrystalline regions, the rotational position of hydroxymethyl groups at the C6 position may be considered as indeterminate or totally nonoriented, which are not identical with those in the crystallites. Therefore it was important to confirm the type of O6 rotational position with respect to the O5 and C4 in a β-glucan chain by employing CP/MAS ^{13}C NMR (Horii et al. 1983). The type of hydroxymethyl conformations is gauche-trans (*gt*), trans-gauche (*tg*), or gauche-gauche (*gg*) at the C6 position in carbohydrates. As for the noncrystalline states, they are considered to be the *gg* conformation (see Figure 6.2).

NOC is prepared by uniaxial stretching of water-swollen cellulose from the N,N-dimethylacetamide (DMAc)/LiCl solution at a draw ratio of 2.0 to provide highly oriented β-1,4-glucan molecular chains of cellulose toward the stretching axis (Togawa and Kondo 1999). When the dissolved cellulose molecules in the DMAc/LiCl system are self-aggregated in water vapor to form a gel, presumably with a minimum amount of restricted engagements among the hydrophobic sites of the ring previously described, it is stretched

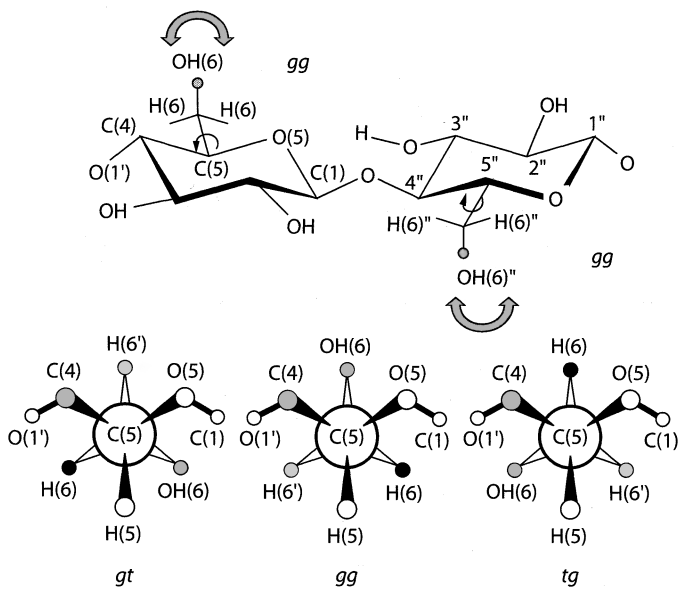

FIGURE 6.2
Schematic diagram of the hydroxymethyl conformations at the C6 position, that is, the orientation of the C6–O6 bond, gauche-trans (*gt*), trans-gauche (*tg*), or gauche-gauche (*gg*) with a cellobiose unit.

to reach NOC. It should be noted that the drawability requires entanglements such as cross-linking, but they are supposed to be minimized. In the present DMAc/LiCl system for NOC preparation, however, slower coagulation using water vapor yielded stable noncrystalline cellulose. The key to maintaining the amorphous or noncrystalline state should be formation of small amounts of the 3D cross-linking network. When the cellulose solution spread on the petri dish is exposed to a saturated water vapor, it turns out to be a gel state with shrinking. The shrinkage is probably due to the interchain hydrogen bonds formed during the coagulation process of cellulose molecules into a sort of network structures. After the solvent was exchanged into water, a transparent water-swollen fixed gel of cellulose (WSC) is obtained. The WSC is composed of approximately 93 wt% water and 7 wt% cellulose. During drawing of the WSC, water retained inside the WSC appeared to bleed out from its surface. The exclusion of excess water from the drawn WSC gel may be attributed to adjoining the cellulose chains between the junction zones, as shown in Figures 6.3a and 6.3b. The junction zone in Figure 6.3a represents the strongly hydrogen-bonded area where even D_2O vapor could not penetrate (Hishikawa et al. 1999). The zone probably plays a role as a cross-linking point in the WSC fixed gel of an initial state for NOC. After drying of the drawn WSC under a stressed state, it showed a decrease in thickness of more than 80% and shrinking in width of more than 60% when compared with the starting sizes of the WSC. The NOC films thus obtained exhibited almost perfect transparency, as much as the coagulated cellulose solution under water vapor atmosphere. This transparency suggests that the NOC should consists of noncrystalline regions.

Figure 6.3 also illustrates structural characteristics of NOC in relation to the situation of OH groups. When NOC is prepared by uniaxial stretching of WSC, the cellulose molecular chains tend to be oriented toward the stretching axis, as described already. Further, the hydroxymethyl groups at the C6 position of the anhydroglucose unit are vertically stuck against the surface, which indicates that the neighboring anhydroglucose ring planes are facing each other. Simultaneously the stuck OH groups in the individual molecular chains are also aligned like tracks along the stretching axis. In contrast, the lateral order of the OH groups among the neighboring chains is not well coordinated because of the slipped molecular chain situation with each other. Therefore the hydrophilic and polarized OH groups are totally oriented as molecular tracks only in the stretching direction across the entire NOC surface. Between the hydrophilic molecular tracks, the hydrophobic phase due to the anhydroglucose plane also appeared alternately, resulting in both hydrophilic and hydrophobic tracks next to each other across the NOC surface. The amphiphilic molecular tracks enhance the unique surface properties of NOC, as described later.

The NOC structure was shown by the high-resolution transmission electron microscopy (TEM) image. The NOC template with molecular ordering is shown in Figure 6.4 (Kondo 2007; Kondo et al., 2001). The high-resolution

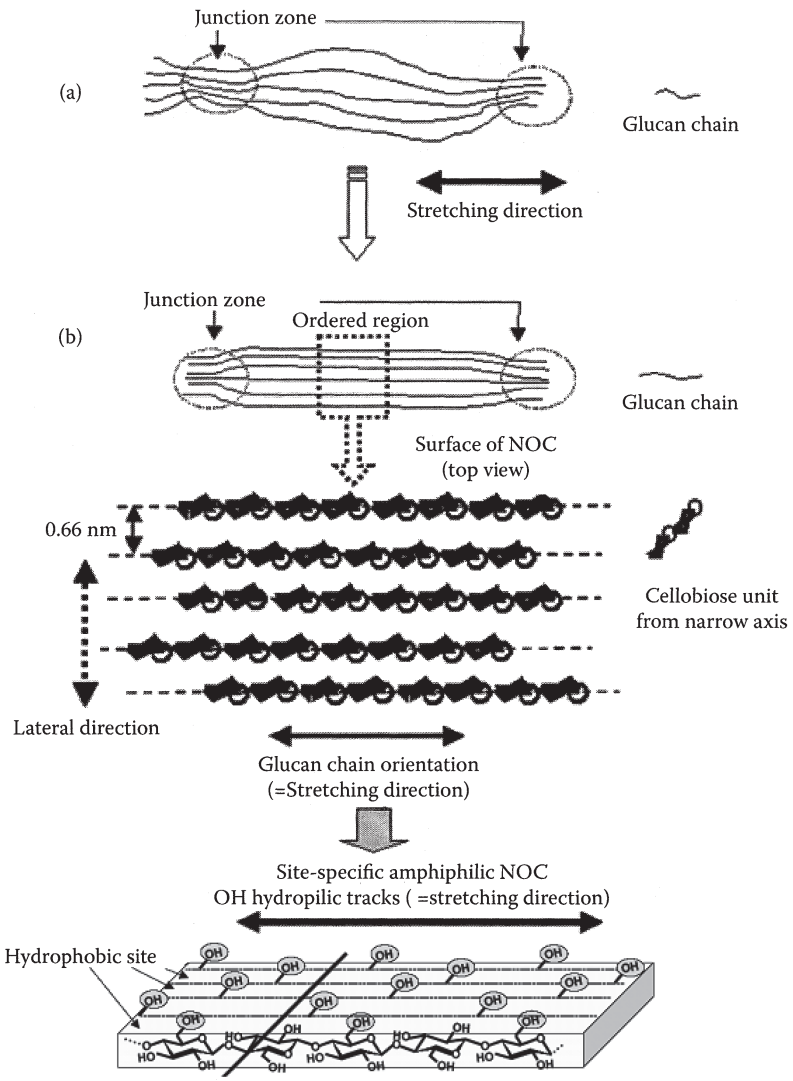

FIGURE 6.3
Schematics of NOC: (a) the initial state before stretching, (b) after stretching, the arrangement of cellulose molecules on the NOC surface.

TEM image shows a preferentially oriented direction on the surface. These observations confirmed the mean width of a single glucan chain corresponding to its known dimensions as viewed from the narrow axis of the anhydroglucose ring. The average chain width was 0.462 nm (standard deviation ±0.0517 nm). Thus the true width seems to be approximately 0.4–0.5 nm when taking into account the negative stain. The average distance between two parallel chains was 0.660 nm (standard deviation ±0.068 nm), which is larger

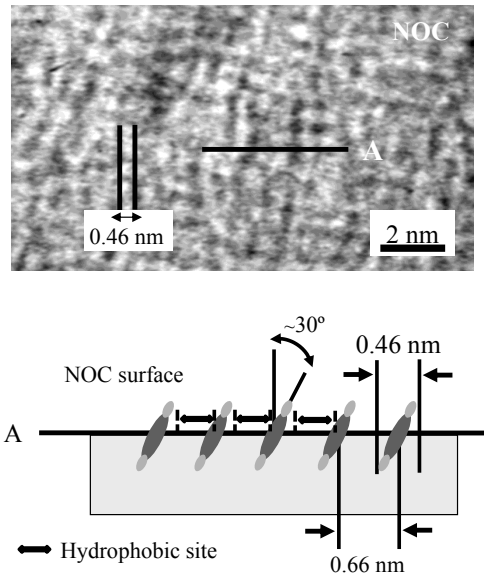

FIGURE 6.4
High-resolution TEM image of NOC, the molecular ordering template, together with the schematic cross-section image perpendicular (lateral direction) to the stretching direction indicating the tilted arrangement of glucan chains. The film was negatively stained by uranyl acetate and spans a region of the copper support grid. Note the individual glucan chains that are separated by an average distance of 0.66 nm (arrows). The arrangement of glucan chains is clearly resolved with a width of 0.46 nm.

than values for any crystalline cellulose. The average width of 0.462 nm from the top view is wider than that of 0.45 nm of the narrow axis in the anhydroglucose ring predicted from the space-filling model. This suggests tilting of the glucose planes of a cellulose molecule with an angle of 29.3° to the vertical axis against the surface of NOC, as shown in the bottom image of Figure 6.4. It should be noted that the static sessile contact angle of a drop of water on the NOC surface is approximately 72°, indicating it is fairly hydrophobic (E. Togawa and T. Kondo, unpublished data). Prior to stretching for NOC preparation, the dried WSC exhibits approximately 50° as the contact angle by the sessile drop method. Thus the surface condition of it is totally altered by stretching to provide tilting of the glucose planes for exposure of the specific hydrophobic site, as shown in Figure 6.4. The hydrophobic phases due to the anhydroglucose plane appear alternately next to the hydrophilic OH tracks, resulting in unique amphiphilic molecular tracks.

Infrared spectroscopic analyses combined with other methods revealed characteristic features of NOC film templates (Hishikawa et al. 2010). The vapor-phase deuteration of the NOC film indicated that the amount of unexchangeable OH groups, 10.6%, of the total OH groups corresponded to the

highly engaged intermolecular hydrogen-bonded domains or the junction zone, as indicated in Figure 6.3a. In addition, polarized Fourier transform infrared spectroscopy (FTIR) combined with the vapor-phase deuteration was enabled to reveal orientation of the cellulose main chains to the stretching direction in both the crystalline domains and the noncrystalline regions of NOC films. The NOC film was also considered to have both the oriented main chains and the nonoriented OH groups as the side chain. This flexible state of the OH groups might further hinder the oriented crystallization in the NOC preparation process and yet induce the unique properties in the surface of the NOC film (Higashi and Kondo 2012; Kondo 2007; Kondo et al. 2002, 2012). In Figure 6.5a, the CP/MAS ^{13}C NMR spectra for NOC samples, as well as amorphous (a noncrystalline state without any preferred orientation) cellulose prepared from cellulose-SO_2-dimethylamine-dimethyl sulfoxide solution (Isogai and Atalla 1991) and CF11 cellulose powder (Whatman International Ltd.) are shown in the range from 50 to 80 ppm where chemical shifts at the C6 position appear. The chemical shift of CF11 appears at 65 ppm, corresponding to *tg* conformation, indicating that CF11 is a native cellulose. Our NOC sample exhibits a broader signal similar to amorphous cellulose within the range of the type of the hydroxymethyl conformation, *gg*, which also supports our suggestion that NOC is noncrystalline even though it is well ordered.

The orientation parameter calculated from wide-angle X-ray diffraction (WAXD) photographs (Figure 6.5b) became 0.88, which indicated a high degree of orientation. However, the crystallinity did not significantly follow the increase of the orientation by stretching (Kondo et al. 2001). Simultaneous orientation and crystallization did not occur as is often seen with crystalline polymers (Ward 1997), which agrees with the infrared (IR) analyses of deuterated NOC samples based on the ratio of the remaining OH groups in the drawn films corresponding to the crystallinity index. The crystallinity was approximately 14.8% and 16.8% before and after stretching, respectively (Kondo et al. 2001; Togawa and Kondo 1999). IR spectra of deuterated samples also supported a low crystallinity of the film based on the ratio of the remaining OH groups in the drawn films that corresponds to the crystallinity index. Figure 6.5b also shows WAXD intensity curves in both the equatorial and meridional directions of NOC (B) together with cellulose II fibers (A). In the equatorial diffraction of NOC, typical crystalline diffraction patterns representing cellulose II were not observed. The diffuse-intensity equatorial profile for NOC indicated that it contains considerably more "amorphous" regions. The meridional scan of WAXD indicates the order along the stretching direction for NOC. Meridional intensities of cellulose are affected by the disorder of the neighboring chains, which is symmetrical for the chain axis. In general, cellulose polymorphs provide almost the same meridional patterns; that is, two strong distinct reflections of the (002) and (004) planes ($2\theta = 17.2°$, $d = 0.516$ nm; $2\theta = 34.7°$, $d = 0.259$ nm, respectively). The present results demonstrate that NOC, which is highly ordered

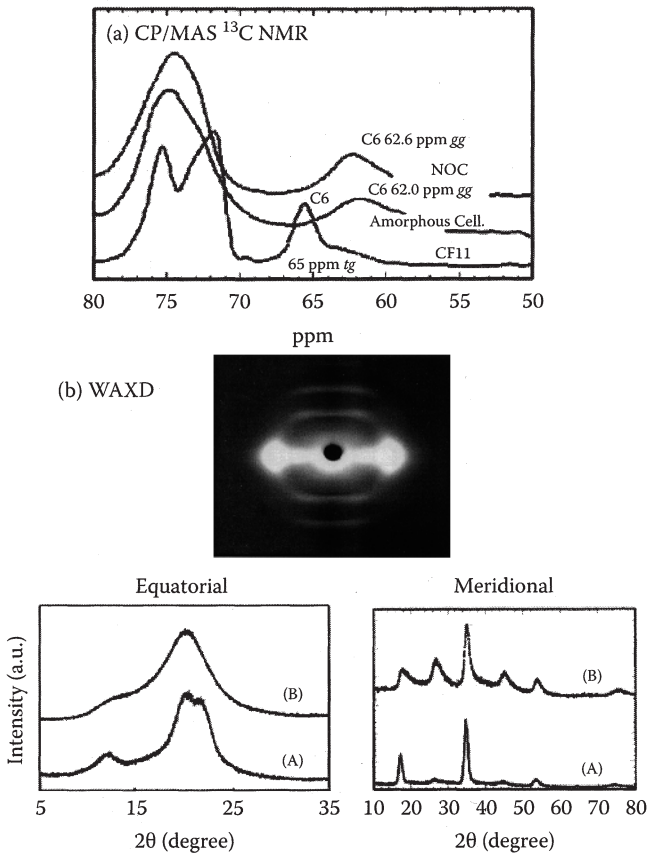

FIGURE 6.5
Characterization of NOC: (a) CP/MAS ^{13}C NMR spectra of NOC, amorphous cellulose, and native cellulose powder (Whatman CF11); (b) WAXD photograph of NOC together with equatorial (left) and meridional (right) intensity curves of the WAXD for cellulose II fibers (A) and NOC (B). The term "a.u." indicates arbitrary unit.

but noncrystalline, gives a totally different profile for the meridional scan, as shown in Figure 6.5b. More reflections were found in the meridional direction when compared with cellulose II crystals. The characteristics are considerable line broadening of the individual meridional reflection peaks in the WAXD profile of NOC. This indicates that the structure of the NOC film along the chain direction may have a certain disorder that causes the ordered, but noncrystalline regions (for more detail, see Kondo 2007). Thus we should consider the states of the structure for NOC to be ordered states that are neither crystalline nor amorphous.

The structural stability of NOC in water was examined. So far, most conventional noncrystalline cellulosics have no orientation in their supermolecular structure, and it is difficult to avoid recrystallization in water, even at

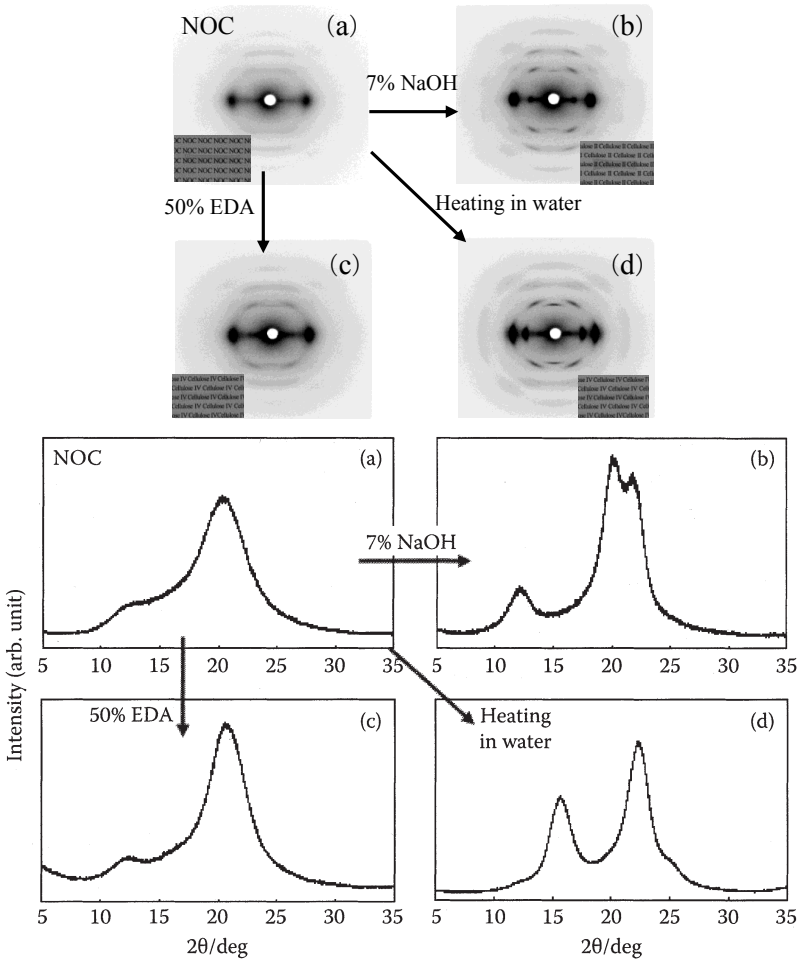

FIGURE 6.6
WAXD images (showing transparent films inserted) and profiles recorded on the imaging plate for NOC film and transformed NOC films: (a) NOC, (b) NOC treated with 7% NaOH, (c) NOC treated with 50% ethylenediamine (EDA), and (d) NOC heated in water at 180°C for 3 h.

room temperature (Isogai and Atalla 1991). Interestingly, the noncrystalline character based on the specific chain orientation of NOC was retained after the treatment in water, even at 50°C for long periods.

Nematic ordered regions, as shown in Figure 6.3b, of the NOC films facilitate transformation into polymorphs. Figure 6.6 shows the X-ray fiber diagrams and photographs of cellulose polymorphs prepared from NOC films, together with the respective equatorial WAXD profiles of the X-ray photographs. Figure 6.6a shows the initial NOC structure as the starting material prior to the crystallization process. Each crystallized structure transformed from NOC (Figures 6.6b–6.6d) had an orientation of crystallites along the

molecular orientation axis of the NOC. Moreover, the obtained films were all transparent, as the photographs in Figure 6.6 indicate. Thus the orientation of molecular chains and the transparency of NOC was maintained, even after crystallization took place. This indicates that the domain sizes of the crystallites were quite small even though they were well oriented along the same molecular orientation direction of the initial NOC film.

The equatorial WAXD patterns of the profiles in Figures 6.6b–6.6d were easily identified as cellulose II, III, and IV, respectively. The results suggest that transformation into each allomorph was completed. It should be noted that all of the transformations were accomplished under milder conditions than the conventional methods reported for the preparation of each allomorphs (Chidambareswaran et al. 1978; Fengel et al., 1995). For example, 16.5% NaOH aqueous solution has thus far been required for transformation from cellulose I to cellulose II when cotton fibers are used as the starting cellulose (Fengel et al. 1995). Using NOC as the starting cellulose assembled state, 7% NaOH was enough for the transformation. In particular, NOC yielded cellulose IV directly by a hydrothermal treatment at more than 100°C without the formation of cellulose III as an intermediate. In a similar manner, we employed cotton cellulose and a commercially available cellophane film as a reference of the starting cellulose to transform into polymorphs under the same conditions used for NOC. However, both cotton and cellophane could never be transformed into each allomorph. The facile transformations are attributed only to the supramolecular structure of NOC, which is well ordered but composed mainly of noncrystalline regions. In fact, the degrees of crystallinity of the three crystallized films from NOC were around 45%. Moreover, our results have demonstrated that such NOC structure in a film material provides, under milder treatments, a facile direct transformation into the oriented films having highly aligned domains of cellulose II, III, and IV allomorphs along the initial orientation in the NOC.

Various Nematic Ordered Templates and Modified NOC

Nematic Ordered Chitin and Chitin/Cellulose Blends

Figure 6.7 shows an image of the chitin template prepared in the same manner as the NOC template and observed with high-resolution TEM as well as atomic force microscopy (AFM) (Kondo et al. 2004, 2012). The two images exhibited the orientation of molecular chains, but they were not clear enough to be estimated. To obtain the distance between individual molecular chains, selected oriented areas (shown in the rectangles of Figure 6.7) of both high-resolution images were at first Fourier transformed to obtain the diffraction images. Then the manipulated diffraction images, as seen in the

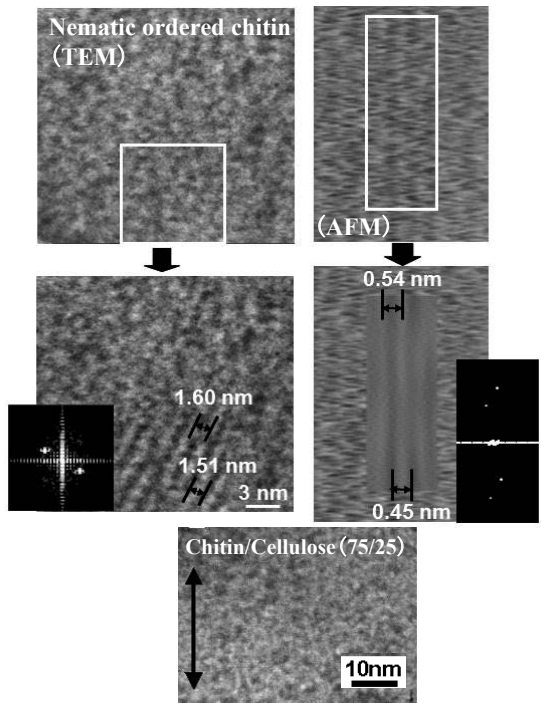

FIGURE 6.7
An image of the chitin template prepared in the same manner as the NOC template: (left upper) observed with high-resolution TEM; (left bottom) an image manipulated by inverse Fourier transformation; (right upper) observed with AFM; (right bottom) an image manipulated by inverse Fourier transformation. The inserted images (both the left and right) are the manipulated diffraction images prior to inverse Fourier transformation. The bottom image is a TEM image of the order structure of the stretched water-swollen gel films from a chitin-cellulose (75-25) blend at a drawing ratio of 2.0. The double arrows indicate the stretching direction. The sample specimens were negatively stained with 2% uranium acetate aqueous solution.

inserted images of Figure 6.7, were inversely Fourier transformed back to the noise-canceled images shown in the bottom images of Figure 6.7. In this way, the average distance between two parallel molecular chains in each image were provided for interpretation. Both observations indicate that the distance between individual chains (1.6 nm for TEM, 0.54 nm for AFM) is larger than the crystalline lattice constant of the *a* axis of α-chitin ([a] 0.474 nm, [b] 1.886 nm, [c] 1.032 nm, $\alpha = \beta = \gamma = 90°$) (Minke and Blackwell 1978). Similar to NOC, in which the glucan chain dimensions are 0.4–0.5 nm viewed from its narrow axis, AFM images with a chain width of 0.45 nm (see Figure 6.7, right) clearly exhibit single molecular chains in the narrow axis on the surface of the chitin template. This means that nematic ordered chitin was achieved, similar to our previous work with cellulose (Kondo et al. 2001). High-resolution TEM images of molecular assembly in the stretched samples

of a chitin-cellulose blend with a composition of 75-25, which was prepared in the same manner as NOC, also exhibit orientation of molecular aggregation, but are not resolved at the individual molecular chain scale (Kondo et al. 2004). The white dots or lines in the chitin-cellulose blend of Figure 6.7 indicate molecular chains or molecular aggregates. Some parts are well oriented parallel to the stretching direction and the molecular aggregates are entirely ordered along the stretching axis.

By image analyses of the TEM image in this figure, the average width and distance between two parallel lines were obtained as 1.38 ± 0.18 nm and 1.65 ± 0.27 nm, respectively. The average line width is narrower than that from the TEM image (1.51 ± 0.27 nm) of nematic ordered pure chitin, indicating that the intermolecular interaction between cellulose and chitin may be engaged. Possibly each molecular chain is facing each other against the surface by a hydrophobic interaction such as van der Waals forces. On the other hand, the average distance between two parallel lines was not significantly different between the two stretched films from pure chitin (1.62 ± 0.21 nm) and the cellulose-chitin blend (1.65 ± 0.27 nm). Therefore it is thought that the cellulose-chitin molecular aggregates in the stretched film are aligned similarly to nematic ordered pure chitin. In addition, these results indicate the presence of another nematic ordered state with a different scale (e.g., nano/micro hierarchical structures) in chitin and the blends with cellulose. (See the more detailed study using WAXD on nematic ordered pure chitin and the blends with cellulose in Kondo et al. [2004] and Kondo [2007].)

Modified NOC

The author proposes in the following sections a novel type of biomineralization process by developing a bifunctional cellulose template (Higashi and Kondo 2012). Namely, the NOC template has been modified into a bifunctional template having a pair of the functions required for biomineralization, resulting in oriented deposition of the biominerals as well as supplying anions in the synthesis. In this case, the new NOC template that is prepared to contain phosphate anions (termed p-NOC) is expected to mediate a unique order patterned deposition of calcium phosphates on the surface by reaction with calcium cations during immersion in a buffer solution.

The modification of NOC is performed as follows: A transparent water-swollen fixed gel of cellulose (WSC) is followed by a procedure using a DMAc/LiCl solvent system, as previously described (Kondo et al. 2001; Togawa and Kondo 1999). The WSC is immersed in phosphate buffered saline (PBS; Sigma-Aldrich) for 1 week to prepare a WSC gel containing phosphate anions. Starting with the gel-like films containing phosphate anions, p-NOC is obtained by uniaxial elongation at a draw ratio of more than 2.0 at room temperature. In the drawing process, the specimen is kept in a wet state by pouring the PBS on the surface of the film. The specimen is then air dried for 24 h

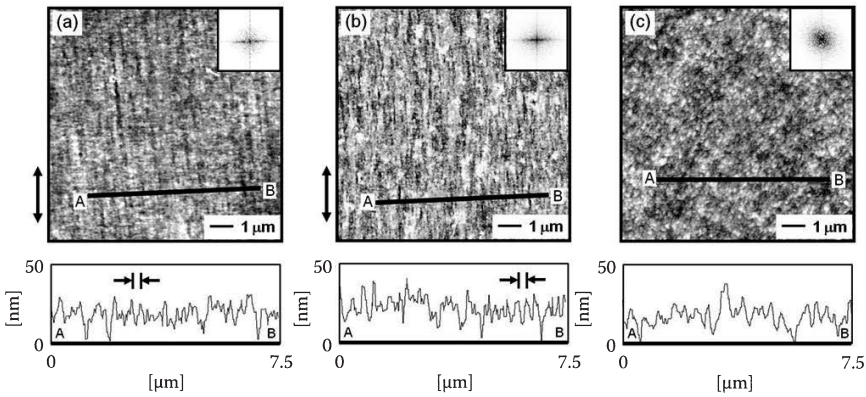

FIGURE 6.8
AFM images of (a) NOC template, (b) p-NOC template, and (c) nonordered cellulose template as a reference for the p-NOC before the reaction with calcium cations. Insets in the upper right indicate the FFT images. The cross-section profiles along the perpendicular (A–B) are shown in the bottom of each figure. In (a and b), the average distances between two parallel lines were (a) approximately 0.17 μm and (b) approximately 0.14 μm. The double arrows indicate the stretching direction.

before being vacuum dried at 25°C for more than 48 h. The AFM images of the p-NOC surface containing phosphate anions together with the original NOC substrate are shown in Figure 6.8. As a reference, a nonordered cellulose template containing phosphate anions is also added (Higashi and Kondo 2012).

In a comparison of the images in Figures 6.8a and 6.8b, the AFM images of the height mode demonstrate that p-NOC containing phosphate anions possesses a well-ordered surface morphology along the stretching direction, similar to the original NOC substrate. Furthermore, the polarized distribution of spots in the two-dimensional fast Fourier transform (2D-FFT) image in Figure 6.8b confirms a high degree of uniaxial orientation on the surface of p-NOC. The average line width was calculated from the cross-section analyses of the height along the A–B line perpendicular to the stretching direction (see the bottom figures in Figure 6.8). The average distance between two parallel cellulose chains was 0.14 ± 0.03 μm in the p-NOC template surface (Figure 6.8b). The line width was similar to that of the original NOC template, 0.17 ± 0.06 μm, as shown in Figure 6.8a, indicating that a physical association of cellulose chains is not interfered even if phosphate anions existed in the p-NOC template. In addition, the negatively polarized surface due to the tracks of OH groups along the molecular orientation is supposed to appear to some extent on the surface of the original NOC (Kondo 2007; Kondo et al. 2001, 2002). Thus, if phosphate anions are contained in NOC templates, then they are likely to be immobilized on the glucose planes only between the OH tracks in the surface that are negatively charged (see Figure 6.9). This means that anions with negative charges could be introduced as the second minus charge into an initially negatively charged film surface. Accordingly,

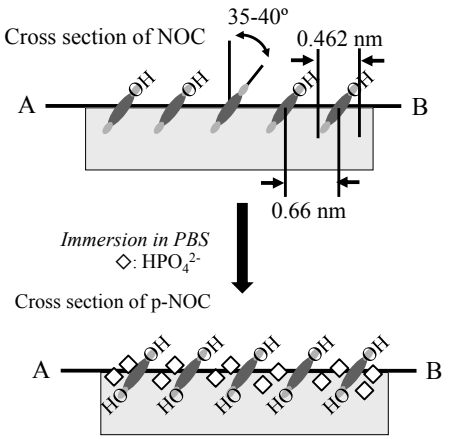

FIGURE 6.9
Schematics of NOC and p-NOC.

the phosphate anions are also supposed to be aligned along the molecular tracks in the newly prepared p-NOC template.

Without stretching of the gel containing phosphate anions, a nonordered structure was observed on the surface, which is confirmed by 2D-FFT images, as shown in Figure 6.8c. By uniaxial stretching of the cellulose gel, it is thought that the p-NOC will have a unique surface morphology similar to NOC that is totally different from the nonordered cellulose template containing phosphate anions. The root mean square (RMS) volumes were calculated from the obtained AFM height images to compare the surface roughness of each template. The RMS values for p-NOC and nonstretched cellulose corresponded to 8.3 nm and 6.2 nm, respectively. Thus p-NOC exhibited a rougher surface than cellulose without stretching.

Exclusive Surface Properties of NOC and Its Unique Applications

Biodirected Epitaxial Nanodeposition on Molecular Tracks of NOC Template

As already described, NOC exhibits several unique properties as a template having the exclusive surface of a nano-/microstructure. That is, the OH groups tend to be oriented as molecular tracks in only one direction across the entire NOC surface. In addition, as shown in Figure 6.4, the hydrophobic sites are supposed to appear alternately next to the OH tracks, resulting in amphiphilic tracks in one direction.

The ordered amphiphilic tracks of hydrophilic OH groups and hydrophobic polarity in NOC can induce an epitaxial deposition of biosynthesized cellulose nanofibers secreted from the Gram-negative bacterium, *G. xylinus*, along the same axis of the tracks in NOC (Kondo et al. 2002). When active *G. xylinus* cells are transferred to the oriented surface, they synthesize cellulose nanofibers parallel to the molecular orientation of the substrate. This is evidenced by direct video imaging of the motion of the bacteria as they synthesize the cellulose nanofiber. The movement of *G. xylinus* in relation to cellulose biosynthesis was reported in 1976 by Brown et al. The cell movement (at a constant rate of 4.5 µm/min at 24°C) is the result of an inverse force imposed by the directed polymerization and crystallization of the cellulose. It is also well known that the bacterium rotates on its own axis. The biodirected epitaxial nanodeposition of secreted fibers was studied over time and under varied conditions, including different substrates. Typically a time course analysis of an NOC template shows a bacterium moving in contact with a stretched NOC substrate, as shown in Figure 6.10. Basically the cells on the NOC template move straight along the molecular tracks. Midway through this series the cell "jumps off" of the oriented substrate and continues to secrete its cellulose nanofiber, but now in the form of a spiral or tunnel structure that is the normal pattern of formation when not in contact with any organized substrate (Thompson et al. 1988). When the interaction between the bacterium and

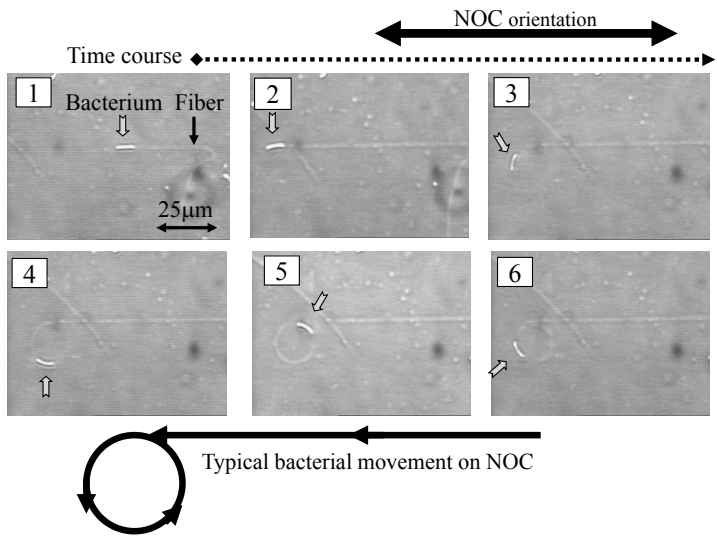

FIGURE 6.10
Successive images showing the motion of a bacterium as it secretes a cellulose ribbon using real-time video analysis. In (1), the bacterium is attached to and synthesizing its cellulose on the monomolecular rail track. In (2), the bacterium has jumped the track and is beginning to change its orientation. In (3–5), the bacterium is generating the first complete spiral. In (6), the bacterium is on the second rotation of a spiral.

the surface of the NOC is strong enough, the bacterium follows the track of the molecular template. As the polymer orientation of the NOC is not necessarily perfect, the bacterium may jump off the track at a structural defect (Figure 6.10-3). After the bacterium leaves the track (Figures 6.10-3–10-6), two forces, the inverse force of the secretion and the close interaction of adjacent microfibrils, affect the bacterium, possibly resulting in the synthesis of a spiral ribbon of microfibrils. In addition, the bacterium begins to rotate on its own axis. This rotation is the visible result of ribbon twisting, which occurs to relieve strain induced by the absence of interaction with the substrate. When the ribbon is assembled in direct contact with the oriented molecular NOC substrate, ribbon twisting is prevented, thus suggesting a control of this oriented solid surface over the final physical interaction of polymer chains immediately after synthesis and during the early stages of crystallization.

Ribbon interaction is more clearly shown by field emission scanning electron microscopy (FE-SEM) in Figures 6.11A and 6.11B. In this experiment, the motion of the same sample is observed using light microscopy and then the sample is prepared for FE-SEM observations. In Figures 6.10a and 6.10b the time course sequence demonstrates an intense, directed nanodeposition that is exclusively linear and without cell rotation as the bacterium follows the track. This is confirmed by the ribbon structure shown by the FE-SEM images in Figures 6.11A and 6.11B, which reveal no twisting and a more perfect alignment with the substrate. Likewise, when the bacterium "jumps off" the track, the cellulose ribbon is twisted (data not shown). Figures 6.11c–6.11f indicate the active *Gluconacetobacter* cells cultured on the oriented surface

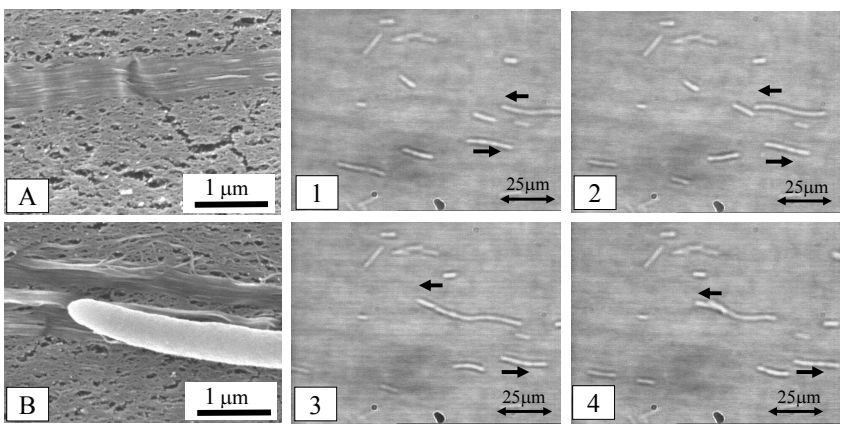

FIGURE 6.11
FE-SEM images of the cellulose nanofiber deposition process. (A, B) Examples of bacteria synthesizing cellulose fibers on the oriented molecular track of NOC. (A) Demonstrates the tight association between the molecular track and the cellulose fiber. In (B), a bacterium shows a flat fiber immediately behind its site of synthesis. (1–4) Successive images showing the motion of a bacterium on a nematic ordered blended film of cellulose and cellulose acetate that has been unixially stretched in the same manner as NOC.

of a blend of cellulose and *O*-methylcellulose with DS 1.6 (50/50 w/w) that has been unixially stretched in the same manner for NOC. The bacteria also tend to follow the molecular tracks on the surface of the oriented cellulosic blend template, similar to the NOC case. In addition, the bacteria exhibit similar linear movements along the molecular tracks on NOC/cellulose acetate (DS 1.7) templates as the NOC. That is, the NOC blends as well as NOC are supposed to show similar unique properties as templates that direct the bacterial movement. When *Gluconacetobacter* cells are placed on an agar surface as a control, their interaction seems to be reduced, and twisted nanofibers are always deposited, also in a random fashion. It should be noted that this regulated movement of the bacterium is not observed in the synthetic polymers having OH groups, such as polyvinyl alcohol, but only in the nematic ordered states of carbohydrate polymers described earlier (Kondo et al. 2002).

Critical Factors in Biodirected Epitaxial Nanodeposition on Molecular Tracks

Hierarchical Order

Figures 6.12a–b show AFM images before and after incubation of *Gluconacetobacter* cells showing fabrication of a 3D architecture along the molecular tracks of NOC as a scaffold. After culturing for 10 h (Figure 6.12b), the height increased by 10 times, to approximately 350 nm, selectively in the stripes on the NOC. This is evidence of the directed close contact between the secreted nanofibers and the molecular tracks on NOC templates. Moreover, the elastic modulus increased slightly from 6.2 ± 0.1 GPa to 6.9 ± 0.0 GPa by patterned fabrication with the secreted cellulose nanofibers on the NOC surface. Presumably the change is mostly influenced by the sufficient strength of NOC as a scaffold when compared with the deposited nanofibers on the above. Here one can observe that the additional layers secreted over time continue to mimic the original orientation initiated in the first deposited layer (e.g., the epitaxial deposition).

Epitaxial Deposition

The adhesion occurs between biosynthesized cellulose microfibrils and the C6 primary OH groups and/or hydrophobic tracks described previously. The important factor for controlling bacterial movements may be close contact and strong interaction between the molecular tracks on NOC and the newly synthesized cellulose microfibrils. A schematic explaining this concept is shown in Figure 6.13. Normally *G. xylinus* secretes a cellulose nanofiber that comprises a microfibril approximately 3.5 nm in width, as shown in Figure 6.13 (left). The microfibrils from the subunit of terminal complexes

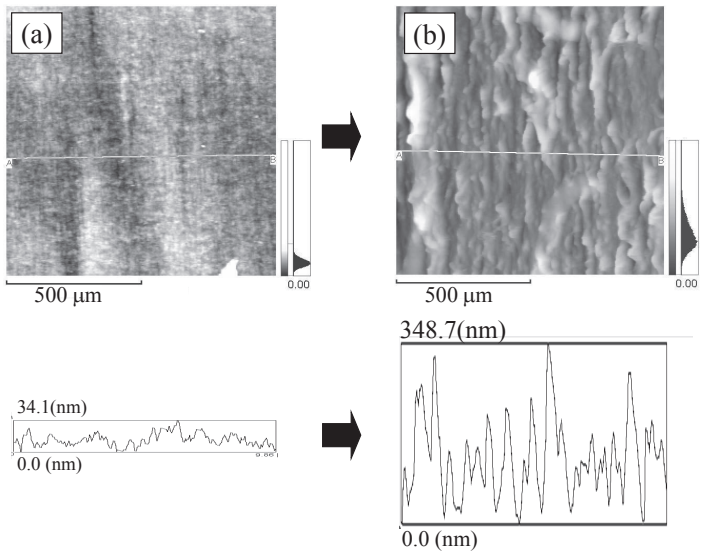

FIGURE 6.12
AFM images (a) before and (b) after incubation of *G. xylinus* on NOC for 10 h in Hestrin–Schramm media.

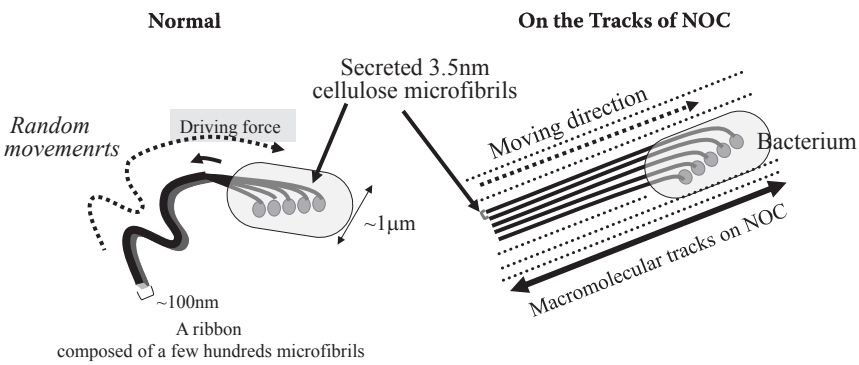

FIGURE 6.13
Schematics of self-assembly of cellulose microfibrils secreted from *G. xylinus* in normal fashion (left) and on the tracks of NOC templates (right). The circles indicate cellulose-synthesizing enzyme subunits linearly arranged across the cell body.

are assembled by interfacial interactions, including hydrogen bonding and van der Waals forces, between the component molecules, resulting in the formation of a ribbon-like cellulose nanofiber approximately 50 nm in width and 10 nm in thickness (Tokoh et al. 1998). In contrast, a cellulose microfibril would be synthesized along the molecular track on the NOC by the strong adhesive effect (Figure 6.13, right). This epitaxial deposition is clearly confirmed by the FE-SEM image of the NOC-altered cellulose ribbons with a

width of 500 nm with splayed microfibrils 7–8 nm apart (see Figure 6.11A and 6.11B) (Kondo et al. 2002).

The amphiphilic molecular tracks on NOC allow close contact with the glucan chains of microfibrils as they are being secreted and crystallized. Thus, in theory, this interaction is predicted to alter the self-assembly of glucan chains into the crystalline microfibril (Benziman et al. 1980; Haigler et al. 1980, 1982; Tokoh et al. 1998; Yamamoto et al. 1996). In fact, alteration of the aggregation of cellulose microfibrils on NOC was demonstrated as described earlier. Such interactions with the substrate alter production of the cellulose ribbon and also the motion of the bacterium, and provide support for the epitaxial nature of cellulose deposition on NOC. Thus nanoscale interactions induce microscale structural changes. Such interactions could be used on a larger scale to selectively modify biopolymers for many applications.

Critical Factors

The adhesion for epitaxial growth of microfibril deposition requires several different critical factors relating to molecular "order" of the substrate. This order is represented by three factors: molecular chain orientation, specific polymer chain conformation, and O6 rotational position with respect to O5 and C4 in a β-glucan chain. The importance of molecular chain orientation is supported by the observation that unstretched NOC does not cause epitaxial deposition. As already described, we believe the C6 hydroxymethyl conformation of NOC is also of importance. Its role is like an anchor for molecular tracks to direct the epitaxial deposition of cellulose nanofibers. The conformation of C6 OH groups is believed to contribute to the crystalline forms, depending on either *gt* (cellulose II) or *tg* (native cellulose). When an NOC with the *gg* hydroxymethyl conformation is crystallized, it is converted to ordered films containing cellulose II crystalline forms with *gt* hydroxymethyl conformation (Togawa and Kondo 2007). When *Gluconacetobacter* is incubated on the crystallized NOC, there is no adhesion of the secreted microbial cellulose nanofibers. The crystallized films do not exhibit the molecular track effect to direct bacterial movements any longer. The same lack of adhesion is observed with substrates prepared from native crystalline cellulose I from *Valonia* (data not shown). In the crystalline samples, the specific polymer chain conformation is changed, and the rotational conformation at C6 is *gt* in crystallized NOC and *tg* in *Valonia* cellulose. Considering this, we conclude that the role of primary OH groups at the C6 position is greater than those of OH groups at the C(2) and C(3) positions. In addition, it is also noted that not only the OH tracks but also the hydrophobic tracks are supposed to appear on the NOC surface, and thus the amphiphilic molecular tracks are critical for regulating the epitaxial deposition of the cellulose nanofibers.

Ordered noncrystalline cellulose (NOC) and related blends have been proven to work very well as templates. Surfaces of nematic ordered chitin also show the adhesive effect, but in an unusual fashion.

The rate and direction of the movement correspond to those of the fiber production. The fibers were reported to be produced at a rate of 2 μm/min at 25°C (Brown et al. 1976). However, *G. xylinus* produced the fiber faster on NOC templates, at a rate of 4.5 μm/min at 24°C. This gap is thought to be due to the strength of the interaction between the biosynthesized fiber and the NOC surface. It is also indicated that the NOC surface promoted the secretion rate of the fibers.

The optimal condition on the templates containing the additives for the culture medium was studied in order to understand the factors influencing the rate of movement of *G. xylinus* accompanied with the secretion of a nanofiber (Tomita and Kondo 2009). The template having a molecular orientation at a higher draw ratio was more effective at enhancing the moving rate. Further, the moving rate may depend on the constituents of the template. The additive, CMC, with a lower DP, was effective at preventing secreted cellulose microfibrils from self-assembling, which resulted in an increase in the rate of movement on the agar substrate. In fact, the Hestrin–Schramm (1954) medium containing 1% CMC with a low DP enhanced the moving rate of the bacterium cultured on the template without orientation. Furthermore, on an NOC template, the Hestrin–Schramm medium containing 1% CMC with a high DP was more effective at increasing in the moving rate. Presumably alignment of the CMC molecules onto the oriented cellulose molecules in the NOC by a strong interaction caused the increase in the moving rate. From the results, the conditions for increasing the moving rate are proposed to employ a flat drawn template with an orientation that can engage with other materials by a strong interaction. Further, supplying an additive to the medium, which prevents self-assembly of secreted cellulose microfibrils, is also effective. Thus understanding how to prevent self-assembly of the secreted microfibrils on the oriented templates could be the easiest way to find an optimal condition for enhancing the fiber production. More importantly, the regulated movement of the bacteria due to the ordered surface of the NOC may trigger the development of a 3D structure of hierarchical architecture from the nano to the micro levels. Therefore, we could regulate the 3D architecture of materials using nanofiber secreted by *G. xylinus* as a building block.

Regulated Patterns of Bacterial Movements Based on Their Secreted Cellulose Nanofibers Interacting Interfacially with Ordered Chitin Templates

When active *G. xylinus* cells are transferred to the nematic ordered chitin surface, they synthesize cellulose nanofibers (i.e., cellulose ribbons) that are not parallel to the molecular orientation of the substrate, unlike the secreted

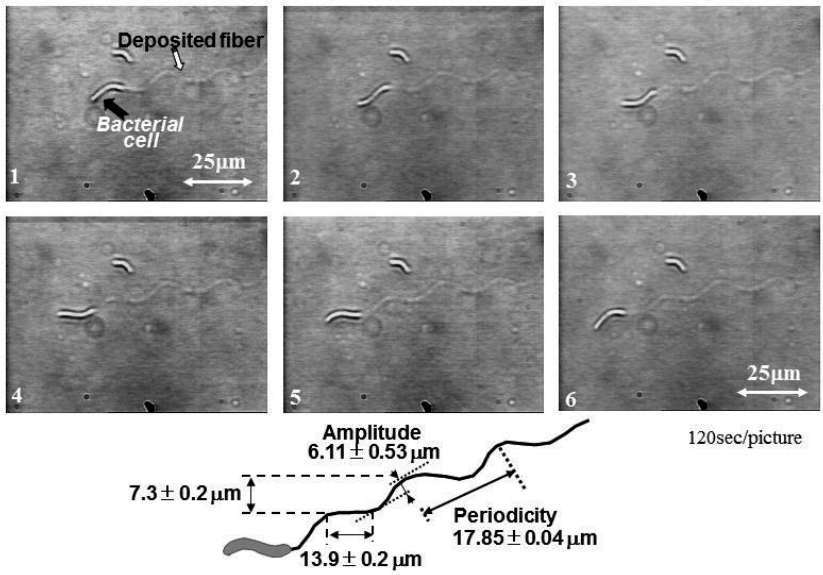

FIGURE 6.14
Successive images showing the motion using real-time video analysis of a bacterium as it secretes a cellulose nanofiber on the nematic ordered chitin template. The bacterium is attached and thereafter is synthesizing the fiber on the molecular tracks in the template showing a "waving" motion pattern.

fibers deposited on NOC templates. Instead, the bacteria begin to follow the molecular tracks, but soon they jump off the track and synthesize their cellulose parallel to neighboring tracks, once again soon jumping off. This "waving" pattern was repeated across the template, as evidenced by direct video imaging of the motion of the bacteria as they secrete the cellulose nanofiber, as shown in Figure 6.14 (Kondo et al. 2012).

Figure 6.14 shows the time course (120 s between each frame) of the waving pattern of movement for a *G. xylinus* cell having a width of 1 μm and a length of 10 μm in length, together with the deposited fiber in the same waving pattern. The time-lapse observation also showed that the cell movement was at a constant rate of 2.05 μm/min (standard deviation ±0.14 μm/min) at 24°C, which is thought to be the result of an inverse force imposed by the directed polymerization and crystallization of the cellulose in the bacterium. The amplitude and periodicity of the waving as indicated in Figure 6.14 was 6.11 ± 0.53 μm and 17.85 ± 0.04 μm, respectively. As seen in the minimum standard deviation in the periodicity of the waving pattern, the movement of the bacterium is fairly periodic and regular. However, the rate of motion on the nematic ordered chitin template was the same as that for cell movements without templates. Furthermore, there was no difference in the rate of movement on the track and off the track, indicating that the interaction of the

nascent cellulose with the nematic ordered chitin template was not as strong as that with the NOC template (Kondo et al. 2002).

In nematic ordered chitin templates, hydrophilic OH groups at the C6 position of the glucopyranose ring and relatively hydrophobic acetamide groups at the C2 position appeared alternately on the surface because of the 2_1 screw axis of the molecular chain, whereas the NOC template provides only OH groups at the C6 position on the surface. The balance of the two substituents strongly affects the strength of the interaction between the surface and secreted cellulose microfibrils. When the contact with the chitin template is not as strong as that for NOC, the biosynthesized individual subelementary fibrils (a few nanometers in width) usually tend to be self-assembled to form a ribbon-type nanofiber with a width of 40–60 nm. The situation when the bacteria secrete cellulose nanofibers cannot be changed without such a strong interaction between the interfaces. Accordingly, the rate of deposition of the fibrils on the nematic ordered chitin template that corresponds to the rate of the bacterial movement did not change from the initial rate without the template (both the moving rates were 2.05 μm ± 5% at 24°C). In contrast, when the interaction was strong enough, as in the case of NOC, the rate of movement was much higher when compared with movements on the templates composed of chitin.

To explain this phenomenon one needs to determine the rate-determining step for both the production of fibers and bacterial movements. In a previous chapter (Tomita and Kondo 2009), it was assumed to be the self-assembly process of biosynthesized subelementary fibrils for forming a cellulose nanofiber. That is, the strong interfacial contact with the template prevented the assembly of the individual subelementary fibrils soon after biosynthesis, resulting in an increase in the rate. This could also cause the release of stress for the enzymatic synthesis of cellulose. As a result, the production of fibers on the NOC template increases, as does the rate of bacterial movement. In fact, we previously found by FE-SEM observations that the bacterial subelementary fibrils extruded by the synthesizing enzymes could not self-assemble on the NOC template to form cellulose nanofibers, later becoming flattened by strongly attaching to the molecular tracks of OH groups on the template surface. This shows the prevention of self-assembly of the subelementary fibrils, and, simultaneously, epitaxial nanodeposition along the molecular track direction on the surface of the template.

The unique patterning of the biodirected nanodeposition process can be also observed by imaging the deposited cellulose nanofibers using FE-SEM correlated with real-time video analysis using light microscopy.

At first, light microscopic observations of the deposited fiber clarified that adherence to the molecular tracks occurred every 13.9 μm (standard deviation ±0.2 μm) as a mean distance along the orientation of the template, as shown in Figure 6.14. Alternating with this parallel movement, the cell "jumped off" the tracks and detoured every 7.3 μm (standard deviation ±0.2 μm) until it became parallel to neighboring tracks, as also indicated in

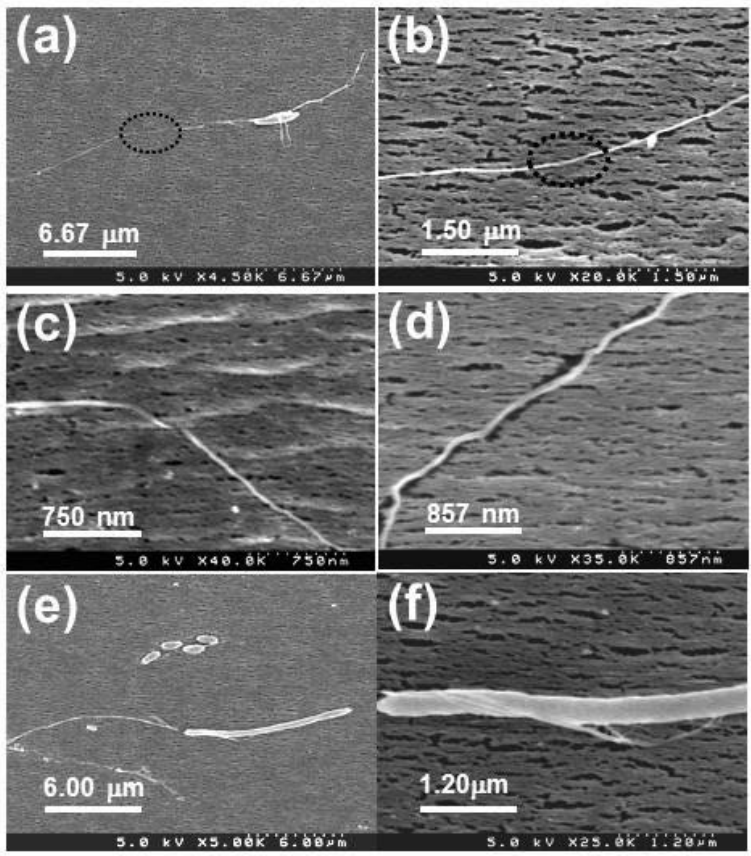

FIGURE 6.15
FE-SEM images of the cellulose nanofiber deposition process. (a–d) Examples of bacteria synthesizing cellulose nanofibers on the oriented molecular tracks of nematic ordered chitin template. (e, f) Examples indicate self-rotation of a *G. xylinus* cell.

Figure 6.14. Once again, soon jumping off, it repeated in the same manner until it stopped moving.

Figure 6.15a shows a bacterium in contact with a nematic ordered chitin template that was moving in a "waving" fashion. During the moving pattern, it deposited a cellulose nanofiber that relatively flattened due to interaction with the nematic ordered chitin prior to the curving pattern in the movement. In the FE-SEM images of Figures 6.15a and 6.15b, the dotted circle indicates the area where the interaction between the fiber and template occurred because the contrast of the image was not clear when compared with other areas of the fiber as assimilated. Thus such an interaction may be a trigger for a change in the direction of the bacterial cell.

After the cell "jumped off" the tracks on the oriented chitin template, it continued to secrete its cellulose ribbon, but now in the form of a twisted

ribbon (Figures 6.15c and 6.15d), which is the normal morphology when not in contact with an ordered substrate. This alternating pattern was observed to repeat as many as 20 times across the entire template.

G. xylinus usually rotates around the self-axis with secretion of a cellulose nanofiber, resulting in twisted cellulose nanofibers. In fact, Figures 6.15c and 6.15d show this rotating movement that was an indication of no interaction of the secreted fiber with the chitin template. Thus Figures 6.15e and 6.15f, which show winding fibers around the bacterium body, confirm self-rotation of the bacterium cell during the detour following jumping off the tracks. Figure 6.15f is an enlarged view of the cell in Figure 6.15e. It is clear that the cell extruded the fiber with twisting, attributed to self-rotation of the cell. These results suggest that the magnitude of interfacial interaction can regulate the waving pattern of bacterial movements and the deposition of nanofibers, which leads to autonomous fabrication of 3D structures with a unique pattern and a controlled growth direction.

With the addition of cellulose as a component for nematic ordered chitin template, the molecular ordering was altered (Kondo et al. 2012). It was found that application of the preparative method for NOC to chitin and cellulose-chitin blends did not permit the formation of nematic ordered states like NOC on the molecular scale, but instead induced a variety of hierarchical nematic ordered states on various scales (Kondo et al. 2004). It was expected that the magnitude of interfacial interactions that occurred with the microfibrils by addition of cellulose as a component would be altered. In the two templates of nematic ordered chitin-cellulose blends of 50-50 and 25-75, the moving patterns were still "waving." However, a remarkable difference appeared depending on the cellulose component ratio. The more cellulose that was added, the smaller the amplitude became—getting close to a linear pattern. This indicates that more cellulose reduces the moving amplitudes into a linear pattern. The moving rate for the individual blend ratios seemed to be within a nonsignificant range.

NOC Templates Mediating Order Patterned Deposition Accompanied by Synthesis of Calcium Phosphates as Biomimic Mineralization

This section briefly introduces an advanced possibility of NOC templates having bifunction (p-NOC) in terms of a novel biomineralization (Higashi and Kondo 2012). As described previously, NOC exhibits a unique property as a scaffold for fabrication of organic hierarchical structures as seen in living things. Recently this concept was extended to fabrication of organic–inorganic hierarchical structures using less energy consumption. The NOC was at first modified into a bifunctional template containing

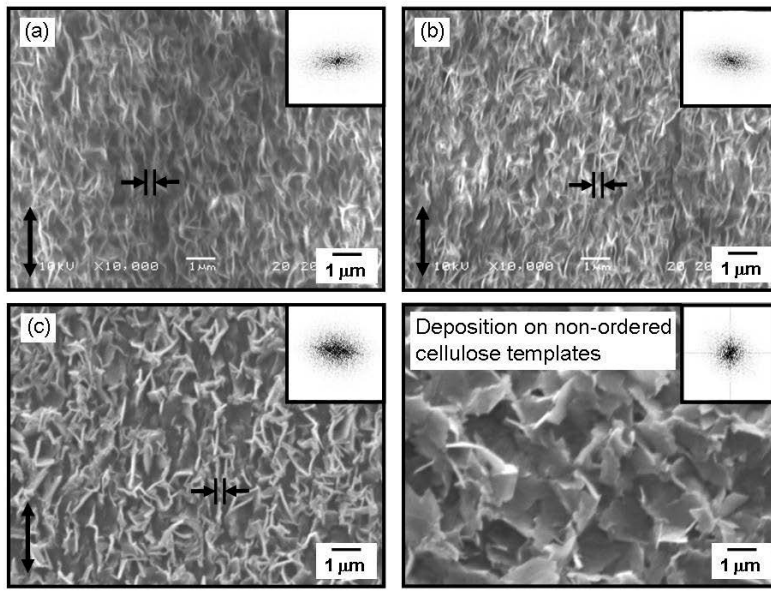

FIGURE 6.16
SEM images of the surface of p-NOC templates after reactions with calcium cations for (a) 0.5, (b) 5.0, and (c) 10 min with the FFT images as insets on the right. The morphology of calcium phosphate deposition on the nonordered cellulose template after the same reaction for 10 min is also displayed as a reference for the p-NOC template. In (a–c), the line width of calcium phosphate was 0.23 ± 0.07 μm, 0.19 ± 0.04 μm, and 0.30 ± 0.08 μm, respectively. The double arrows indicate the stretching direction.

phosphate anions for biomineralization, resulting in induction of oriented deposition of calcium phosphates as well as supplying phosphate anions.

The surfaces of both p-NOC and nonordered p-cellulose templates as a reference for the p-NOC after reaction with the calcium cations in the buffer solution were analyzed using SEM observation. Figures 6.16a–6.16c show the surface morphological change of the p-NOC with calcium cations. Large amounts of calcium phosphates were formed over the surface of the p-NOC template after the reaction with calcium cations. In addition, the assembled pattern of the deposited minerals was well arranged along the molecular orientation of the p-NOC surface. The FFT images corresponding to each SEM image in Figures 6.16a–6.16c indicate that the longer the reaction time, the poorer the orientation of the deposition of calcium phosphate aggregates became. The average distance between the oriented mineral lines (n = 50) was approximately 0.23 ± 0.07 μm (a), 0.19 ± 0.04 μm (b), and 0.30 ± 0.08 μm (c). These values were larger than those between the apparent tracks due to cellulose molecular chains on the p-NOC surface (see Figure 6.8b; approximately 0.14 ± 0.03 μm [n = 50]). The FFT image with a polar distribution confirms better orientation of the lines as shown in Figures 6.16a–6.16c, when compared with the nonordered cellulose template in Figure 6.16.

The calcium phosphate did not take any ordered shape on the surface of the nonordered p-cellulose template as a reference for p-NOC, although large amounts of calcium phosphate were also formed over the surface (see the SEM image in the bottom right of Figure 6.16). In addition, the FFT image of the nonordered cellulose template exhibited randomly distributed spots, indicating that the deposition pattern of the calcium phosphate on the nonordered template was not induced in a preferable manner. This result strongly suggests that the p-NOC surface encourages uniaxially oriented deposition accompanied by synthesis of the calcium phosphate. It was obvious that the surface orientation of the p-NOC template mediated the orientation of the calcium phosphate, because of the correspondence with each other. However, the orientation of the inorganic deposits on the p-NOC surface tended to be reduced with the longer reaction time (Figure 6.16a–6.16c).

Furthermore, the particle size of the calcium phosphate on the p-NOC template was smaller than that on the nonordered p-cellulose template. It was presumably because 3D mineral deposition and its growth tended to be inhibited by the close contact of the uniaxially oriented cellulose molecular chains on p-NOC. The deposition of calcium phosphate was mostly limited to the orientation direction of the cellulose molecular chain, and thereby the calcium phosphate was supposed to be arranged along the stretching direction of p-NOC. It was a similar mechanism to biomineralization with inhibition of the 3D crystalline growth and the arrangement of the mineral shape mediated by oriented scaffolds such as collagen or chitin (Kato et al. 2002; Rho et al. 1998). Thus the p-NOC template is a biomimic template in terms of inducing the orientation of calcium phosphate, as well as a phosphate anion supplier (Higashi and Kondo 2012).

The Future

In biological systems, skeletal materials such as cell walls, bones, and shells are made primarily of a nanoscale building block of polysaccharides, proteins, and inorganic salts. The assembly of these building blocks facilitates the production of a hierarchical framework structure. The formation dynamics observed in this NOC could be applicable to the design of nanoscale, controlled, hierarchically structured materials with specific properties. We have employed a biological system combined with a polymer platform having an NOC-like surface in order to directly fabricate hierarchically ordered materials from the nano level up to the micron level. Such a surface property would greatly extend the possibilities of cellulose use to new areas. Thus, if a nano-/micropatterned film having similar surface characteristics as an NOC can be fabricated, the 3D-patterned materials will be built up by mediation of the cellulose or related scaffolds, and thereby widely appreciated and used.

Acknowledgments

The author thanks R. M. Brown, Jr., at the University of Texas, Austin, for research collaboration. W. Kasai and Y. Tomita, in my laboratory at Kyushu University, are also acknowledged. This research was supported partly by a Grant-in-Aid for Scientific Research (nos. 22380097 and 23658146) from the Japan Society for the Promotion of Science (JSPS).

References

Benziman, M., C. H. Haigler, R. M. Brown, Jr., A. R. White, and K. M. Cooper. 1980. Cellulose biogenesis: polymerization and crystallization a coupled processes in *Acetobacter xylinum*. *Proc. Natl. Acad. Sci. USA* 77:6678–6682.

Brown, R. M., Jr., J. H. M. Willison, and C. L. Richardson. 1976. Cellulose biosynthesis in *Acetobacter xylinum*: visualization of the site synthesis and direct measurement of the in vivo process. *Proc. Natl. Acad. Sci. USA* 73:4565–4569.

Chidambareswaran, P. K., S. Sreenivasan, N. B. Patil, H. T. Lokhande, and S. R. Shukla. 1978. Fine structural changes in native and mercerized fibrous cellulose brought about by ethylenediamine and methyl alcohol. *J. Appl. Polym. Sci.* 22:3089–3099.

Drexler, K. E. 1992. *Nanosystems: molecular machinery, manufacturing, and computation*. New York: Wiley Interscience.

Fengel, D., H. Jakob, and C. Strobel. 1995. Influence of the alkali concentration on the formation of cellulose II. Study by X-ray diffraction and FTIR spectroscopy. *Holzforschung* 49:505–511.

Haigler, C. H., R. M. Brown, Jr., and M. Benziman. 1980. Calcofluor white alters the in vivo assembly of cellulose microfibrils. *Science* 210:903–906.

Haigler, C. H, A. R. White, R. M. Brown, Jr., and K. M. Cooper. 1982. Alteration of in vivo cellulose ribbon assembly by carboxymethylcellulose and other cellulose derivatives. *J. Cell. Biol.* 94:64–69.

Hesse, S., and T. Kondo. 2005. Behavior of cellulose production of *Acetobacter xylinum* in 13C-enriched cultivation media including movements on nematic ordered cellulose templates. *Carbohyd. Polym.* 60:457–465.

Hestrin, S., and M. Schramm. 1954. Synthesis of cellulose by *Acetobacter xylinum*. 2. preparation of freeze dried cells capable of polymerizing glucose to cellulose. *Biochem. J.* 58:345–352.

Higashi, K., T. and Kondo. 2012. Nematic ordered cellulose templates mediating order-patterned deposition accompanied with synthesis of calcium phosphates. *Cellulose* 19:81–90.

Hishikawa, Y., E. Togawa, Y. Kataoka, and T. Kondo. 1999. Characterization of amorphous domains in cellulosic materials using a deuteration-FTIR monitoring analysis. *Polymer* 40:7117–7124.

Hishikawa, Y., E. Togawa, and T. Kondo. 2010. Molecular orientation in the nematic ordered cellulose film using polarized FTIR accompanied with a vapor-phase deuteration method. *Cellulose* 17:539–545.

Horii, F., A. Hirai, and R. Kitamaru. 1983. Solid-state ^{13}C-NMR study of conformations of oligosaccharides and cellulose conformation of CH_2OH group about the exo-cyclic C-C bond. *Polym. Bull.* 10:357–361.

Isogai, A., R. H. and Atalla. 1991. Amorphous celluloses stable in aqueous media: regeneration from SO_2-amine solvent systems. *J. Polym. Sci. Polym. Chem.* 29:113–119.

Kato, T., A. Sugawara, and N. Hosoda. 2002. Calcium carbonate-organic hybrid materials. *Adv. Mater.* 14:869–877.

Kondo, T. 2007. Nematic ordered cellulose: its structure and properties. In: *Cellulose: Molecular and Structural Biology*, ed. R. M. Brown, Jr. and I. M. Saxena, 285–306. Dordrecht: Springer.

Kondo, T., W. Kasai, and R. M. Brown, Jr. 2004. Formation of nematic ordered cellulose and chitin. *Cellulose* 11:463–474.

Kondo, T., W. Kasai, M. Nojiri, Y. Hishikawa, E. Togawa, D. Romanovicz, and R. M. Brown, Jr. 2012. Regulated patterns of bacterial movements based on their secreted cellulose nanofibers interacting interfacially with ordered chitin templates. *J. Biosci. Bioeng.* 114:113–120.

Kondo, T., M. Nojiri, Y. Hishikawa, E. Togawa, D. Romanovicz, and R. M. Brown, Jr. 2002. Biodirected epitaxial nanodeposition of polymers on oriented macromolecular templates. *Proc. Natl. Acad. Sci. USA* 99:14008–14013.

Kondo, T., E. Togawa, and R. M. Brown, Jr. 2001. "Nematic ordered cellulose": a concept of glucan chain association. *Biomacromolecules* 2:1324–1330.

Minke, R., and J. Blackwell. 1978. The structure of α-chitin. *J. Mol. Biol.* 120:167–181.

Rho, J. Y., L. Kuhn-Spearing, and P. Zioupos. 1998. Mechanical properties and the hierarchical structure of bone. *Med. Eng. Phys.* 20:92–102.

Taton, T. A. 2002. Bio-nanotechnology: two-way traffic. *Nature Mater.* 2:73–74.

Thompson, N. S., H. M. Kaustinen, J. A. Carlson, and K. I. Uhlin. 1988. Tunnel structures in *Acetobacter xylinum*. *Int. J. Biol. Macromol.* 10:126–127.

Togawa, E., and T. Kondo. 1999. Change of morphological properties in drawing water-swollen cellulose films prepared from organic solutions: a view of molecular orientation in the drawing process. *J. Polym. Sci. B Polym. Phys.* 37:451–459.

Togawa, E., and T. Kondo. 2007. Unique structural characteristics of nematic ordered cellulose: stability in water and its facile transformation. *J. Polym. Sci. B Polym. Phys.* 45:2850–2859.

Tokoh, C., K. Takabe, M. Fujita, and H. Saiki. 1998. Cellulose synthesized by *Acetobacter xylinum* in the presence of acetyl glucomannan. *Cellulose* 5:249–261.

Tomita, Y., and T. Kondo. 2009. Influential factors to enhance the moving rate of *Gluconacetobacter xylinus* due to its nanofiber secretion on oriented templates. *Carbohydr. Polym.* 77:754–759.

Ward, I. M. 1997. Introduction. In: *Structure and Properties of Oriented Polymers*, 2nd ed., ed. I. M. Ward, 1–15. London: Chapman & Hall.

Yamamoto, H., F. Horii, and A. Hirai. 1996. In situ crystallization of bacterial cellulose II. Influences of different polymeric additives on the formation of celluloses Iα and Iβ at the early stage of incubation. *Cellulose* 3:229–242.